*Submit to JPC, Special Issue*

# A competition of several energy transport initiation mechanisms defines the ballistic transport speed

Sithara U. Nawagamuwage, Layla N. Qasim, Xiao Zhou, Tammy X. Leong, Igor V. Parshin, Janarthanan Jayawickramarajah, Alexander L. Burin, Igor V. Rubtsov*

Department of Chemistry, Tulane University, New Orleans, Louisiana 70118, United States
*corresponding author: irubtsov@tulane.edu

**Abstract**

Ballistic regime of vibrational energy transport in oligomeric molecular chains occurs with a constant, often high, transport speed and high efficiency. Such transport regime can be initiated by exciting a chain end group with a mid-IR photon. To better understand the wavepacket formation process, two chemically identical end groups, azido groups with normal, $^{14}N_3$-, and isotopically substituted, $^{15}N_3$-, nitrogen atoms, were tested for wavepacket initiation in compounds with alkyl chains of $n$ = 5, 10, and 15 methylene units terminated with a carboxylic acid (-a) group, denoted as $^{14}N_3C$*n*-a and $^{15}N_3C$*n*-a. The transport was initiated by exciting the azido moiety stretching mode, the $\nu_{N\equiv N}$ tag, at 2100 cm$^{-1}$ ($^{14}N_3C$*n*-a) or 2031 cm$^{-1}$ ($^{15}N_3C$*n*-a). Opposite to expectation, the ballistic transport speed, was found to decrease upon $^{14}N_3 \rightarrow {}^{15}N_3$ isotope editing. Three mechanisms of transport initiation of a vibrational wavepacket are described and analyzed. The first mechanism involves direct formation of a wavepacket via excitation with IR photons of several strong Fermi resonances of the tag mode with the $\nu_{N=N}$ + $\nu_{N-C}$ combination state, while each of the combination state components are mixed with delocalized chain states. The second mechanism relies on vibrational relaxation of an end-group-localized tag into a mostly localized end-group state that is coupled strongly to multiple delocalized states of a chain band. Harmonic mixing of $\nu_{N=N}$ of the azido group with $CH_2$ wagging states of the chain permits a wavepacket formation within a portion of the wagging band, suggesting a fast transport speed. The third mechanism involves vibrational relaxation of an end-group-localized mode into chain states. Two such pathways were found for the $\nu_{N\equiv N}$ initiation: the $\nu_{N=N}$ mode is relaxing efficiently into the twisting band states and low-frequency acoustic modes and the $\nu_{N-C}$ mode relaxes into the rocking band states and low-frequency acoustic modes. The contributions of the three initiation mechanisms in the ballistic energy transport initiated by $\nu_{N\equiv N}$ tag are evaluated quantitatively and related to the experiment. We concluded that the third mechanism dominates the transport in alkane chains of 5-15 methylene units initiated with the $\nu_{N\equiv N}$ tag and the wavepacket generated predominantly at the $CH_2$ twisting band. The isotope effect of the transport speed is attributed to a larger contribution of the faster wavepackets for $^{14}N_3C$*n*-a and/or to different breadth of the wavepacket within the twisting band. The study offers a systematic description of different transport initiation mechanisms and discusses the requirements and features of each mechanism. Such analysis will be useful for designing novel materials for energy management.

**Key words:** intramolecular energy transport, 2DIR, RA 2DIR, dual-frequency, vibrational wavepacket, Fermi resonance, $^{15}N$ isotope, optical phonons

TOC graphics:

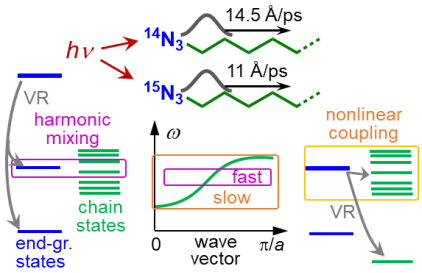

## 1. Introduction

Ballistic energy transport via acoustic phonons is prevalent in ordered materials such as crystals and can occur to large distances. The amount of energy transferred via wavepackets made of acoustic phonons is limited by the thermal energy, $k_BT$, which is too small to significantly influence chemical processes. In recent studies ballistic energy transport via covalent bonds of linear oligomeric chains was discovered to occur via optical chain bands, thus delivering substantially larger energy quanta to distances exceeding 60 Å[1-4] and featuring much higher efficiency compared that in diffusive energy transport.[5-8] Oligomeric chains feature a range of chain bands differing in energy and bandwidth. The bandwidth of a chain band determines the mean group velocity of the wavepacket supported by the band.[9] The ballistic through-chain transport was initiated via excitation with a mid-IR photon a vibrational mode at the end group, which then transferred its energy into the chain, initiating the transport. The energies of the end-group modes tested for ballistic transport range from 2100 $cm^{-1}$ (azido group stretch)[1] to 1650-1750 $cm^{-1}$ (carbonyl groups in carboxylic acid, ester, succinimide ester, and amide),[9-10] 1500 $cm^{-1}$ (amide II mode of an amide),[10] and ~1300 $cm^{-1}$ (azido group stretch).[9] It was found that selection of the end group mode used to initiate the transport determines which chain band transfers energy, thus determining the transport speed and efficiency. For example, ballistic transport via alkane chains, initiated by an azido-group stretching mode at 2100 $cm^{-1}$, occurs with the speed of 14.5 Å/ps (1.45 km/s), while the speed is 8.0 Å/ps when initiated by a carbonyl stretching mode at 1710-1820 $cm^{-1}$,[9] and only 4.2 Å/ps when initiated with the amide-I mode of an amide end group.[10] Earlier reports by Troe[11-12] and Dlott[13-14] groups indicated the presence of ballistic transport via alkane chains.

Although ballistic transport was reported via several oligomeric chains, PEG,[15] alkane,[9, 12] perfluoroalkane,[16] and p-phenylene,[17] the transport initiation mechanisms were not discussed systematically. At the same time, the central role of the transport initiation process became apparent as the end-group properties define which band or portion of the band is involved in the through-chain transport, thus defining the transport speed and efficiency. This study is inspired by the interest in designing molecular systems with faster and more efficient energy transport. Such systems have a high potential as novel materials suitable for energy management, delivering energy to remote regions, including energy transport against thermal gradient, and materials for molecular electronics. The energy quanta delivered via optical chain bands are large enough to be used for initiating remotely low-barrier chemical reactions. Approaches to direct and alternate ballistic transport by external stimuli,[10, 17] may result in creating energy transport switches.

Instead of changing the nature of the end group, drastically changing its properties, in this study we vary the frequency of the end group vibrational mode via isotope editing of the end group atoms, $^{14}N_3$- $\rightarrow$ $^{15}N_3$-, targeting different portions of the alkane chain bands and thus expecting different transport speeds. Using previously reported dispersion curves for alkane chains,[9] a higher transport speed was expected for the $^{15}N_3$- initiation.

The paper reports experimental results of energy transport via linear alkyl chains of 5 ,10, and 15 methylene groups terminated with an isotopically edited azido group and a carboxylic acid group, $^{15}N_3C$*n*-a (Section 3.1). The experiments were performed using relaxation-assisted two-dimensional infrared (RA 2DIR) spectroscopy where the excess energy arrival from the initially excited end-group mode (tag) to the site of the end group at the opposite chain end (reporter) was recorded as a time dependence of the tag-reporter cross peak amplitude.[7] Systematic description of the ballistic transport initiation mechanisms is given in Section 3.2. Sections 3.3-3.6 discuss different mechanisms of transport initiation in $N_3C$*n*-a, describing vibrational relaxation pathways of the tag and its relaxation daughter modes and the coupling strength among the end-group and chain states. In the Discussion section we compare different mechanisms of transport initiation offering strategies to design compounds for achieve high efficiency of energy delivery and high transport speed.

## 2. Experimental details

***2DIR measurements***. A comprehensive description of a fully automated dual-frequency three-pulse echo 2DIR instrument with heterodyne detection is presented elsewhere.[18] In brief, a Ti:sapphire laser producing 1.5 W power at 1 kHz repetition rate, 800 nm wavelength, and 80 fs pulse duration (Libra, Coherent) was used to pump a computer-controlled dual optical parametric amplifier (OPA, Palitra-duo, Quantronix). Two pairs of Signal and Idler pulses generated by OPA were directed to two computer-controlled difference frequency generation units (DFG; NIR Quantronix) to generate mid-IR pulses tunable in the frequency range from 500 to 5000 $cm^{-1}$, featuring a pulse energy ranging from 1.0 to 10 μJ. A fully automated 2DIR instrument features the sensitivity of better than $10^{-4}$ $cm^{-1}$ in measured anharmonicities, which is achieved by a combination of a closed-loop phase stabilization to better than 70 as, phase cycling, and spectral interferometry. The automatic frequency tuning from 800 to 4000 $cm^{-1}$ is achieved by implementing a mid-IR beam direction stabilization schematic (<50 μrad deviations)[19] and a schematic for setting the phase-matching geometry for mid-IR beams at the sample.[18] The spectral width of the mid-IR pulses was ∼150 $cm^{-1}$ and the instrument response function was ∼140 fs. The 2DIR measurements were performed by scanning the delay between the first two mid-IR pulses $\tau$ of the same DFG unit at a fixed waiting time *T*, which is the delay between the second and third pulses and recording the heterodyned spectrum in the frequency range of interest ($\lambda \rightarrow \omega_t$) for every $\tau$. Fourier transformation along $\tau$ results in the $\omega_\tau$ axis in the 2DIR spectrum, shown as ordinate. A typical 2DIR spectrum contained ∼250 points along the $\tau$ direction and took 1−3 min to acquire. For the RA 2DIR measurements, the 2DIR spectra were recorded for each waiting time, which was scanned with nonconstant delay steps ranging from 100 fs at small waiting times up to 5 ps at large waiting times. Typical waiting-time dependences contain 40−50 points along *T*, which takes 1−2 h to acquire.

***Sample preparation.*** A series of compounds featuring an isotopically edited azido end group, alkyl chain on three lengths of *n* = 5, 10, 15, and carboxylic acid terminating moiety, denoted as $^{15}N_3C$*n*-a (Fig. 1A), was preparade according to the procedure reported previously for $^{14}N_3C$*n*-a, except isotopically labeled sodium azide ($Na^{15}N_3$, 97% $^{15}N$, Berry & Associates/ICON Isotopes) was used as the reagent.[2] FTIR and 2DIR measurements were performed in a sample cell made of 1 mm thick $CaF_2$ windows and a 50 μm Teflon spacer at room temperature, 22 ± 0.5°C.

***DFT calculations.*** DFT calculations were performed using Gaussian 09 suite. Geometry optimization, vibrational mode analysis and anharmonicity calculations were executed using B3LYP functional and 6-311+G(d,p) basis set in dichloromethane(DCM) solvent described with a PCM method. Vibrational relaxation pathways of the end-group states were computed using theoretical approach reported in references [20-21]. The method uses DFT-computed anharmonic coupling constants of an isolated molecule to computes third-order relaxation pathways. The relaxation pathways from several excited azido group states were performed for compounds with *n* = 1, 5, terminated with a hydrogen atom of 2000 amu instead of the carboxylic acid moiety denoted as $^{15}N_3C$*n* and $^{14}N_3C$*n*.

Vibrational couplings between the modes of the azido moiety and chain states were evaluated for both $^{14}N_3C$*n* and $^{15}N_3C$*n* compounds with *n* = 1 and 5 using previously reported approach where the atomic masses of the end group atoms are changing smoothly causing the end-group frequency change, and the Hessian matrix is diagonalized for each mass point.[9] As the end-group frequency passes the resonance with a chain states, a frequency jump occurs equal to the $2\beta$, where $\beta$ is the interaction energy of the end-group and chain state.[9]

## 3. Results

### *3.1. 2DIR measurements of the energy transport*.

Both high-frequency modes of the azido moiety, denoted as $\nu_{N\equiv N}$ and $\nu_{N=N}$, are affected significantly by the $^{14}N_3$- $\rightarrow$ $^{15}N_3$- isotope editing (see Section S1 in Supporting Information). The frequency of the $\nu_{N\equiv N}$ mode, found at 2100 cm$^{-1}$ in $^{14}N_3C$*n*-a is red shifted in $^{15}N_3C$*n*-a by 69.2 cm$^{-1}$ (Fig. 1B). The frequency of the N=N mode, found at ca. 1270 cm$^{-1}$ in $^{14}N_3C$*n*-a, is also red shifted in $^{15}N_3C$*n*-a by ca. 45 cm$^{-1}$ (Fig. 1B inset).

2DIR cross peak spectra, focusing at the $\nu_{N\equiv N}$ / $\nu_{C=O}$ cross peak, were measured for $^{15}N_3C$*n*-a by tuning the first two IR pulses to excite the $\nu_{N\equiv N}$ tag mode at 2031 cm$^{-1}$ and the third and local oscillator (LO) pulses to access the $\nu_{C=O}$ reporter mode at 1709 cm$^{-1}$ (Fig. 1C). The cross-peak spectra were measured for a range of waiting times, *T*, and waiting time kinetics were constructed by integrating the 2DIR spectra over the cross-peak area and plotting the resulting amplitude as a function of the waiting time (Fig. 1E). The results for $^{14}N_3C$*n*-a are shown in Figure 1D, taken from reference [9]. The traces show a rise with the waiting time increase, associated with the energy transport from the tag to the reporter site. The maximum in the kinetic trace, occurring at $T_{max}$, corresponds to the maximum energy delivered; the following decrease in the cross-peak amplitude is associated with the cooling of the reporter site into the solvent. To determine the $T_{max}$ value for each compound, the traces were fitted with an asymmetric double sigmoidal function (see Fig. S1 in Supporting Information for details). Mean $T_{max}$ values were determined by averaging three measurements per compound (see Section S2 in Supporting Information). The resulting $T_{max}$ values were plotted as a function of the through-bond chain length, determined as a sum of all C-C bond lengths of the chain (Fig. 2A). The dependence was fitted with a linear function and the transport speed, *V*, was evaluated as an inverse slope of the fit function. The energy transport speed along the chain in $^{15}N_3C$*n*-a was found at 11.0 $\pm$ 1.5 Å/ps, which is slower than 14.5 $\pm$ 0.5 Å/ps, reported for $^{14}N_3C$*n*-a.[9]

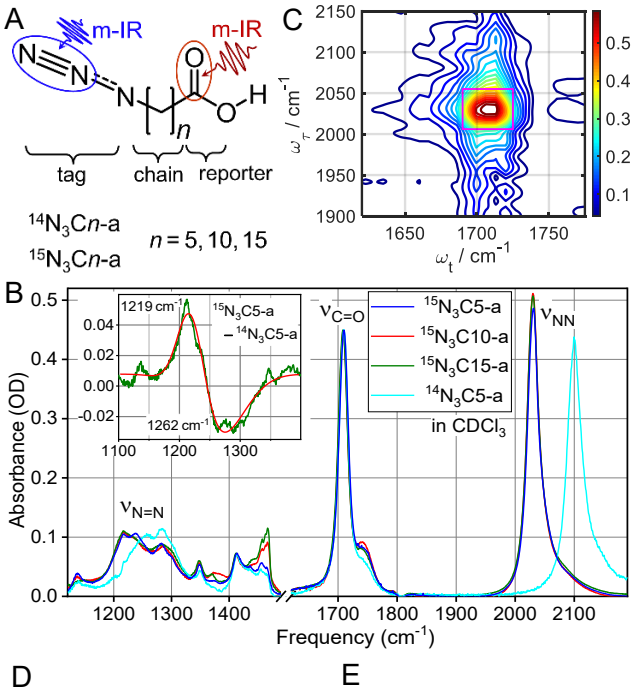

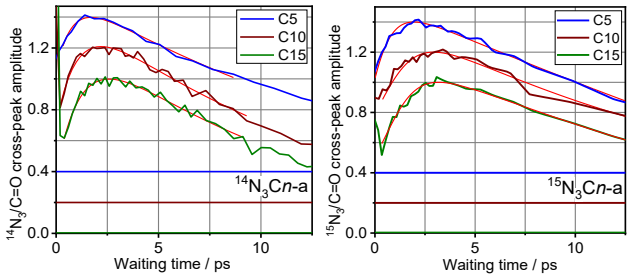


**Fig 1**. A. Molecular structure of the used compounds. B. Linear absorption spectra of the $^{15}N_3$C5-a, $^{15}N_3$C10-a, $^{15}N_3$C15-a, and $^{14}N_3$C5-a in $CDCl_3$, normalized for the carbonyl peak at $\nu_{C=O}$ at ca. 1709 cm$^{-1}$. Two azido-group vibrational modes denoted as $\nu_{N\equiv N}$ (2100 cm$^{-1}$ in $^{14}N_3$C$n$-a and 2031 cm$^{-1}$ in $^{15}N_3$C$n$-a) and $\nu_{N=N}$ (~1250 cm$^{-1}$) are labeled. Inset shows the $\nu_{N=N}$ difference spectrum: $^{15}N_3$C5-a – $^{14}N_3$C5-a and its fit with two Gaussian functions. C. 2DIR spectrum showing the $\nu_{N\equiv N}$ / $\nu_{C=O}$ cross peak for $^{15}N_3$C15-a at $T$ = 3.1 ps. D-E. Waiting-time dependences for the $\nu_{N\equiv N}$ / $\nu_{C=O}$ cross peak for $^{14}N_3$C$n$-a (D)[9] and $^{15}N_3$C$n$-a (E) for $n$ = 5, 10, and 15. Notice that the graphs are spaced vertically, and zero horizontal lines are shown with matching colors. Fitting curves with an asymmetric double sigmoidal function are shown with red lines.

Note that this result is opposite to the prediction of a higher speed with $^{15}N_3$- transport initiation. The expectation was based on the calculations that the $\nu_{N=N}$, a daughter mode of $\nu_{N\equiv N}$ relaxation, matches the portion of the dispersion curves of both $CH_2$ wagging and twisting chain bands which feature higher group velocities (see Section S3 in SI).

It is also notable that longer $T_{max}$ times are observed for $^{15}N_3$C$n$-a compared to $^{14}N_3$C$n$-a (Fig. 2A); the $T_{max}$ values obtained from linear extrapolation to zero chain length differ by ca. 0.5 ps. The increase in $T_{max}$ suggests that the energy injection into the chain occurs slower in $^{15}N_3$C$n$-a.

Presence of different wavepackets featuring different speeds is expected for both isotopes. Faster moving wavepackets contribute the most at the rising portion of the waiting time trace. To inspect contributions of faster wavepackets, the transport speed was also evaluated based on the initial portion of the waiting time traces, the $T_{0.8}$ values, determined as the time the trace reached 0.8 fraction of its maximum amplitude (Fig. 2B).[17, 22] The obtained speed is higher than the $T_{max}$-based speed (Fig. 2B inset) by a factor of 1.6-1.8.

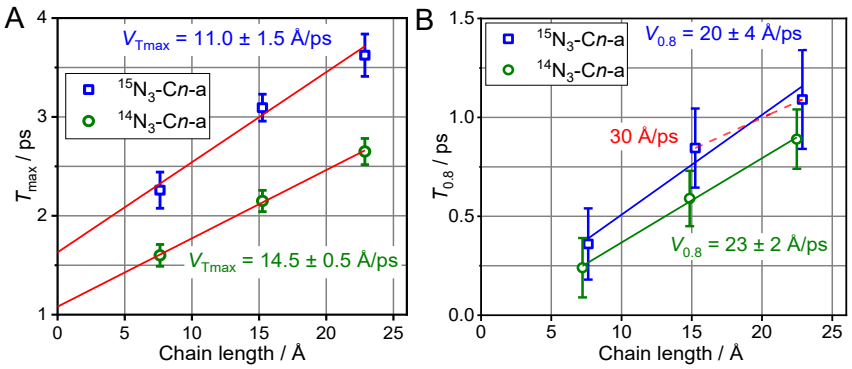


**Fig. 2**. $T_{max}$ (A) and $T_{0.8}$ (B) values as a function of chain length for the two series of compounds: $^{14}N_3$C$n$-a and $^{15}N_3$C$n$-a with $n$ = 5, 10, and 15. Linear fit lines are shown with red color and the corresponding transport speeds obtained from the fits are shown with data matching colors.

Theoretical analysis of the energy injection process was performed for both end groups. The analysis focused on the relaxation channels of the tag ($\nu_{N\equiv N}$) and its relaxation daughter modes ($\nu_{N=N}$ and $\nu_{N-C}$), coupling of the daughter modes and the chains states and Fermi resonances of the tag. We first present a systematic description of different mechanisms of wavepacket initiation.

### *3.2. Mechanisms of Wavepacket Formation.*

Wavepacket initiation by an excited end-group-localized mode requires energy transfer from the end group to the chain states. Different mechanisms of wavepacket excitation in the chain are possible, relying on different extent and order of interaction between the end-group modes and the chain states, as shown in Figure 3. Without losing generality, we consider the tag that is end-group localized and frequency isolated, so it is not harmonically mixed with any chain state. Nevertheless, the tag mode can be anharmonically coupled to other states via Fermi resonances (FR). If strong Fermi resonances occur among the tag and combination bands involving chain-band states, the combination bands will gain IR intensity through intensity borrowing from the tag (Fig. 3A). It is possible to have multiple Fermi resonances involving a range of chain states, as reported for the azido end group.[23] Such combination bands can be excited directly with a photon and can, under certain conditions, form a wavepacket within the chain states.

Another mechanism of wavepacket formation involves vibrational relaxation of the tag into daughter states at least one of which is strongly (harmonically) coupled to the chain states, $\beta_{\text{end gr.}}$ (Fig. 3B). Strong coupling among a daughter mode and a few chain states results in their mixing. Vibrational relaxation, local in nature, excites in this case a superposition of delocalized chain states, such that they involve local motion at the sites nearest to the end group – a wavepacket. The spectral width of the wavepacket is defined by the coupling strength among the end-group daughter mode and the chain state localized at the adjacent methylene site, $\beta_{\text{end gr./ch.}}$, in relation to the coupling within the chain, $\beta_{\text{ch.}}$. If the coupling strength is comparable or larger than the chain band width, $\beta_{\text{end gr.}} \geq \beta_{\text{ch.}}$, all states of the band will be involved in the wavepacket. The transport speed of such wavepacket corresponds to the mean speed of the chain band. If $\beta_{\text{end gr.}} < \beta_{\text{ch.}}$, only a portion of the chain states that is resonant with the end-group mode will participate in the wavepacket. Such wavepacket will feature a group velocity characteristic to a specific portion on the chain band dispersion curve at the frequency of the chain state, not the mean speed supported by the whole band. The spatial size of any wavepacket is defined by the number of chain states involved in the superposition. For the cases with smaller $\beta_{\text{end gr./ch.}}$, longer chains are required to achieve a spatially sharp wavepacket.

Another mechanism of wavepacket formation involves vibrational relaxation of the end-group mode into chain states (Fig. 3C). Local nature of the relaxation process derives from proximity of the involved states for strong coupling.[24-26] Therefore, strong anharmonic coupling of the end-group mode and the local mode at the first chain site is require for efficient relaxation. Anharmonically driven relaxation will excite a local chain mode, which represents a wavepacket in the basis of delocalized chain states. The strength of the anharmonic coupling determines the spectral width of the wavepacket and its spatial sharpness, similar to case B.

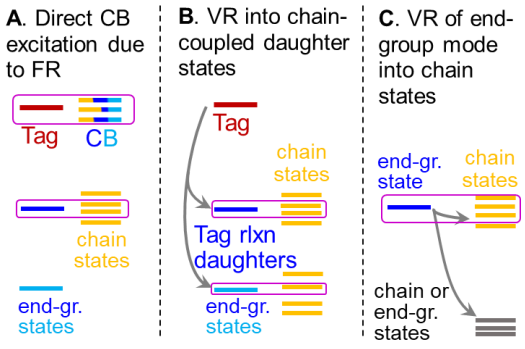


**Fig. 3.** Mechanisms of ballistic transport initiation by an excited end-group-localized vibrational mode. Magenta boxes indicate the couplings required for wavepacket initiation.

In the next section we will consider transport initiation with $\nu_{N\equiv N}$ in $^{14}N_3Cn$-a and $^{15}N_3Cn$-a to identify which mechanism is contributing the most. To identify the differences and similarities in the transport, computational results are presented for compounds with both isotopes. First, we consider a possibility of mechanism B, inspecting the relaxation pathways of the tag and the extent the daughter modes of the tag relaxation involve the chain states.

### *3.3. Vibrational Relaxation Pathways for the $\nu_{N\equiv N}$ Tag.*

We computed the rates of intramolecular vibrational energy redistribution (IVR) pathways using a recently developed theoretical approach.[20-21] To determine vibrational frequencies and anharmonic force constants, DFT anharmonic computations were performed using Gaussian-09 suite[27] for the $^{14/15}N_3$-$(CH_2)_5$-$^{2000}H$ compounds, denoted as $^{14}N_3C5$ and $^{15}N_3C5$, where a large mass for the chain terminating hydrogen was used to decouple its motion from other motions in the compounds. In agreement with previous reports for $^{14}N_3$- initiation,[9, 23] the $\nu_{N\equiv N}$ relaxation predominantly populates a combination band of modes $\nu_{N=N}$ and $\nu_{N-C}$ (Fig. 4A,B), which accounts for >90% of all relaxation channels for both isotopes. To efficiently create a wavepacket in the chain upon the tag relaxation, the relaxation daughter states need to be harmonically mixed with more than one chain state of the same chain band (mechanism B). The $\nu_{N=N}$ daughter state frequency matches the $CH_2$ wagging (W) and twisting (Tw) chain bands (Fig. S2 in SI), while $\nu_{N-C}$ is located within the rocking (Ro) band (Fig. S4 in SI).

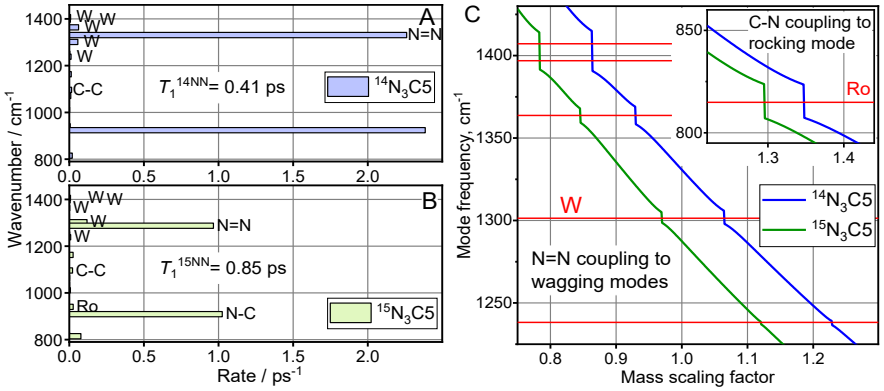


**Fig. 4.** Relaxation pathways for the tag mode, $\nu_{N\equiv N}$, computed for $^{14}N_3C5$ (A) and $^{15}N_3C5$ (B). C. $\nu_{N=N}$ mode frequency of $^{14}N_3C5$ (blue) and $^{15}N_3C5$ (green) as a function of mass scaling factor for the N atoms of the azido group. Horizontal red lines show the frequencies of the wagging chain states. Inset shows the $\nu_{N-C}$ mode frequency as a function of mass scaling factor, indicating its coupling with the rocking state at 815 cm$^{-1}$.

To evaluate the coupling strength of the $\nu_{N=N}$ mode with the wagging and twisting modes of the chain, we scanned the masses of the nitrogen atoms of the azido moiety in increments of 0.01 amu and computed the normal modes for every mass using the Hessian matrix obtained via DFT normal mode analysis.[9] When, as a result of mass change, the frequency of $\nu_{N=N}$ passes that of the chain state, W or Tw, a jump of the mode predominantly residing on the azido group ($\nu_{N=N}$) occurs. The magnitude of the frequency jump equals to $2\beta_{N=N/W}$ or $2\beta_{N=N/Tw}$, where $\beta$ is the respective interaction energy. The computations performed for $N_3C1$ resulted in $\beta_{14N=N/W}$ = 10 cm$^{-1}$, $\beta_{15N=N/W}$ = 8.4 cm$^{-1}$, and $\beta_{N=N/Tw}$ <0.1 cm$^{-1}$ for both isotopes. Similar results were obtained for $N_3C5$, although the observed coupling was different for different wagging states (Figure 4C) due to different contributions at the first methylene site in different wagging normal modes; this contribution is the highest at ca. $1/\sqrt{n}$ for the normal modes featuring the highest wave vectors, where $n$ is the number sites. Note that equal site contributions require cyclic boundary conditions.

Therefore, $\nu_{N=N}$ is harmonically mixed with wagging modes, but only within a rather narrow resonance window of about $\pm 2\beta_{N=N/W}$. The pattern of $\nu_{N\equiv N}$ relaxation pathways confirms the result: in addition to the relaxation pathway to $\nu_{N=N}$ (Fig. 4A), there is a pathway in $^{15}N_3C5$ to a single wagging state, which is shifted by ca. 15 $cm^{-1}$ from $\nu_{N=N}$, and two pathways in $^{15}N_3C5$ to wagging states that are shifted by ca. 25 $cm^{-1}$ from $\nu_{N=N}$. These pathways gain their efficiencies due to mixing of $\nu_{N=N}$ with formally wagging states of the chain. As the site energy gap is larger than $\beta_{N=N/W}$, the mixing is partial. The other wagging states of the chain are further away from $\nu_{N=N}$ and do not feature significant $\nu_{N=N}$ contributions. As a result of small density of chain states in $N_3C5$, the $\nu_{N\equiv N}$ relaxation populates mostly the end-group-localized $\nu_{N=N}$, although a small amplitude wavepacket is also created on the wagging states. The chain state density increases with the chain length increase. For efficient formation of the wavepacket, at least two wagging states need to be found within the $2\beta_{N=N/W}$~20 $cm^{-1}$ window at the frequencies around $\nu_{N=N}$. To satisfy this requirement, the chain length should be ca. 22 and 19 unit long for normal and isotopically substituted compounds. Even for the longest experimentally assessed chain of $N_3C15$-a, two wagging states will not be efficiently excited via mechanism B, suggesting that the influence of such wavepacket will likely be small for the overall energy transport process. A rather high speed is expected for such wavepacket, reaching 40 Å/ps for $^{14}N_3C5$, as the fastest portion of the wagging band will be involved, not the whole band. Essentially the same speed is predicted for $^{15}N_3C5$, either for the wagging band constructed of harmonic, of anharmonic chain states (see Section S3 in SI).

The coupling among $\nu_{N\text{-}C}$ and rocking band states, $\beta_{N\text{-}C/Ro}$, evaluated in a similar way to $\beta_{N=N/W}$, was found to be about 8 $cm^{-1}$ (Fig. 4C inset). The density of rocking states at ca. 900 $cm^{-1}$ is the smallest within the band, corresponding to the highest group velocity of the rocking band, exceeding 65 Å/ps. To have two rocking states separated by $2\beta_{N\text{-}C/Ro}$~16 $cm^{-1}$ for their efficient mixing with $\nu_{N\text{-}C}$, the chain should consist of 44 methylene units. The longest experimentally assessed chain, $N_3C15$-a, is almost three times shorter, which allows to conclude that formation of a wavepacket on rocking states via mechanism B in negligible for these chains. Therefore, vibrational relaxation of $\nu_{N\equiv N}$ remains mostly local to the azido moiety and will not create efficiently a wavepacket on wagging, twisting, or rocking states via mechanism B.

Next, we consider relaxation pathways of the 1st-tier daughters, $\nu_{N=N}$ and $\nu_{N\text{-}C}$, and a possibility of a wavepacket formation via their relaxation into chain states (mechanism C).

### *3.4. Vibrational Relaxation Pathways of $\nu_{N=N}$*

The $\nu_{N=N}$ mode lifetime, computed for both isotopes in $N_3C5$, is very short at 0.20 ps ($^{14}N$) and 0.18 ps ($^{15}N$). Three groups of daughter modes account for 95% of all pathways: all $CH_2$ twisting modes (36.5 rate percent for $^{14}N$ and 50 rate percent for $^{15}N$), NNN bending mode overtone, $\delta_{NNN}$, (35% for $^{14}N$ and 29% for $^{15}N$), and $\nu_{N\text{-}C}$ (23% for $^{14}N$ and 17% for $^{15}N$), Figure S5 in SI. The $\delta_{NNN}$ mode frequency, ~600 $cm^{-1}$, is too low to populate any optical chain bands in the following relaxation process. Excitation of the $\nu_{N\text{-}C}$ mode will be considered in the next section as $\nu_{N\text{-}C}$ is also a daughter mode of $\nu_{N\equiv N}$ relaxation.

The $\nu_{N=N}$ mode relaxation pathways populate multiple twisting chain states in $^{14}N_3C5$ and $^{15}N_3C5$, as shown in Figure 5A,B. Red horizontal lines show the location of the $\nu_{N=N}$ states for respective isotopes. While all twisting states feature appreciable rates and the wavepacket formation seems possible, an additional requirement has to be satisfied to form a wavepacket rather than populating individual states with no specific phase relations characteristic for a wavepacket. The third-order relaxation process involves a parent mode ($\nu_{N=N}$, mode *i*), one of the twisting modes (*j*), and a low frequency mode (*k*). The relaxation process of mode *i* will create a wavepacket only if multiple chain states *j* become populated for the same mode *k*. On the other hand, if different *k* states are involved for different chain states *j*, individual chain states will be excited, not a wavepacket. Five low-frequency *k* modes are involved in the relaxation process. Two of them, modes #49 and #51, result in the strongest rates across all twisting

states (Fig. 5C,D). These two decay channels are characterized by a sufficiently strong third order interaction and involve all twisting chain states spread over a range over 160 cm$^{-1}$ in frequency. Relaxation channels involving both low-frequency modes will generate wavepackets in the twisting bands. They represent ca. 95% of all relaxation channels into twisting-band states for both $^{14}N_3C5$ and $^{15}N_3C5$ (Fig. 5C,D), so the wavepacket formation is efficient. Essentially the whole twisting band is involved in the wavepacket, so the transport speed can be estimated as the mean group velocity for the band: $\langle V_{gr} \rangle = \frac{a}{\pi}\int_0^{\pi/a}\frac{\partial\omega}{\partial q}dq$,[9] computed at 10.4 Å/ps (Fig. S2 and Table S2 in SI).

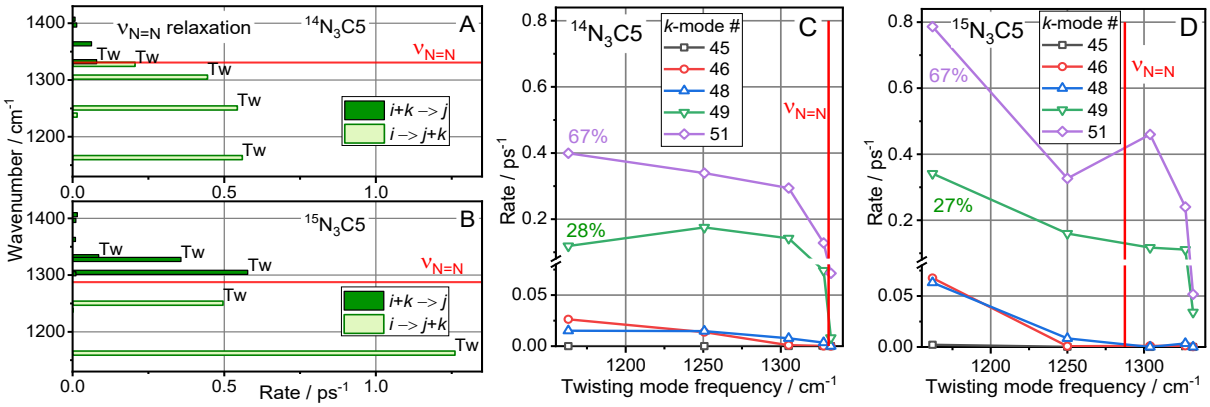


**Fig. 5.** Relaxation pathways of $\nu_{N=N}$ populating twisting modes of the chain, computed for $^{14}N_3C5$ (A) and $^{15}N_3C5$ (B) (see complete set of data in Fig. S5 in SI). Red horizontal lines show the position of $\nu_{N=N}$ for each isotope. C-D. Individual relaxation channels populating the twisting band states for $i \rightarrow j+k$ and $i+k \rightarrow j$ processes where $i$ denotes $\nu_{N=N}$, $j(k)$ denotes one of the twisting modes, and $k$ is a low-frequency mode involved in the IVR step. The points for same $k$ values are connected. The frequencies of the $k$ modes showing significant contributions are 25 (#51), 60 (#49), 81 (#48), 135 (#46), and 148 cm$^{-1}$ (#45).

### *3.5. Vibrational Relaxation Pathways for $\nu_{N-C}$*

The $\nu_{N-C}$ mode lifetime was computed at 0.78 ps for $^{14}N_3C5$ and 0.75 ps for $^{15}N_3C5$. The relaxation pathways involve predominantly the rocking states of the chain (Fig. 6A,B), which account for 72.3 and 76.1 rate percent, respectively. Note that all rocking states are populated significantly, although not evenly. To check if common relaxation process exists to each rocking modes and the same low-frequency mode, we analyzed individual third-order pathways of $\nu_{N-C}$ relaxation, shown in Fig. 6C,D. Five low-frequency modes ($k$ = 45, 46, 48, 49, 51) are involved in the $i \rightarrow j+k$ and $i+k \rightarrow j$ processes, where $i$ denotes $\nu_{N-C}$ and $j$ is one of the rocking band states. The pathways involving $k$ modes 45, 46, and 48 populate a single rocking state and cannot form a wavepacket. $k$ modes 49 and 51 populate more than one rocking states and will form a wavepacket – localized chain excitation at the azido side.

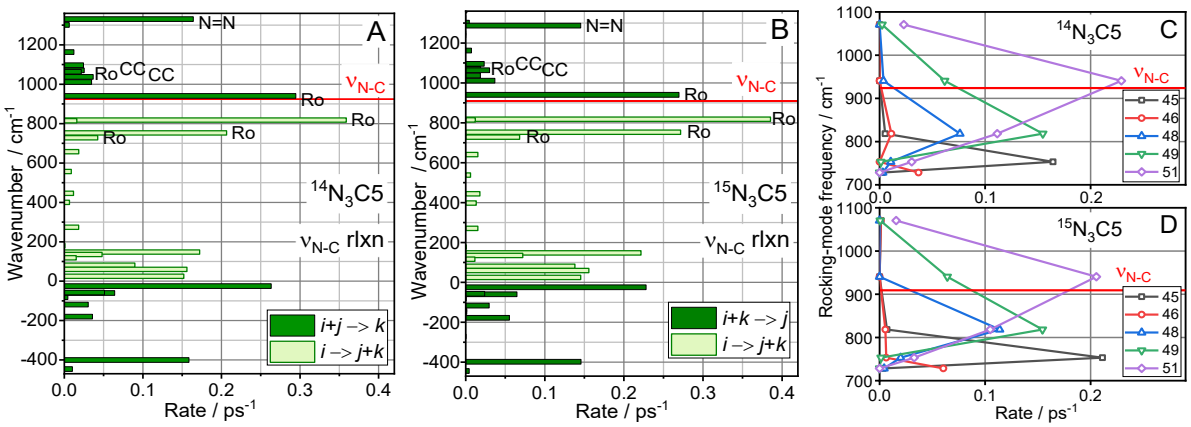


**Fig. 6.** All relaxation pathways of the $\nu_{N-C}$ mode for $^{14}N_3C5$ (A) and $^{15}N_3C5$ (B). The majority of the pathways populate rocking modes of the chain (Ro). Red horizontal lines show the position of $\nu_{N-C}$ for each isotope. C-D. Individual relaxation channels populating the rocking band states for $i \rightarrow j+k$ and $i+k \rightarrow j$ processes where $i$ denotes $\nu_{N-C}$, $j$($k$) denotes one of the rocking modes, and $k$ is a low-frequency mode involved in the IVR step. Points for the same $k$ values are connected. The frequencies of the $k$ modes showing significant contributions are 25 (#51), 60 (#49), 81 (#48), 135 (#46), and 148 $cm^{-1}$ (#45).

The speed of such wavepacket is expected to be extremely high at ca. 67 Å/ps, as the fast portion of the rocking band is involved. Interestingly, the yield of the wavepacket formation with modes 51 and 49, is rather high at 57 and 52% of all relaxation channels into rocking modes for $^{14}N_3C5$ and $^{15}N_3C5$, respectively. Despite rather high predicted efficiency, such high speeds have not been clearly observed experimentally, possibly due to the following reasons: 1) A large spatial size of the wavepacket is expected as a small number of chain states is involved. Large wavepacket size will likely reduce the efficiency of its relaxation to the reporter site as its participation at the last chain site is diminished by broadening. Note, however, that the quality of the wavepacket will increase for longer chains, as more states will be covered by the strength on the involved nonlinear interaction, which is ca. 50 $cm^{-1}$. The rocking sate frequencies are low, which could result in their faster relaxation, although not confirmed experimentally. 2) It is difficult to experimentally tell apart such fast transport from a non-resonant signal appearing at $T$~0 ps, especially if slower but more efficient transport pathways are present. Note that the time to pass a C15 chain for such wavepacket is 0.35 ps, which is only 2-fold longer than the instrument response time (Fig. S6B in SI) and is much smaller than the experimental $T_{max}$ and even $T_{0.8}$ values (Fig. 2B). The difference in the speeds determined from $T_{max}$ and $T_{0.8}$ indicates contributions of faster transport processes, which likely include the transport via the rocking band (Fig. 2B). Note that other chain bands, such as $\nu_{C-C}$ and scissoring, are found to be much less populated via the first two tiers of $\nu_{N\equiv N}$ relaxation and are not expected to participate in the energy transport initiated by $\nu_{N\equiv N}$.

***3.6. Wavepacket Formation via Direct Excitation of $\nu_{N\equiv N}$ Fermi Resonances (Mechanism A).*** Fermi resonance among the $\nu_{N\equiv N}$ fundamental and the combination band of $\nu_{N=N}$ and $\nu_{N-C}$ modes is strong, resulting in significant intensity borrowing. Moreover, the Fermi resonances were shown to be a major reason of a large $\nu_{N\equiv N}$ transition width, observed even in nonpolar solvents.[23] Both states of the combination state are involved in mixing with the chain states, wagging for $\nu_{N=N}$ and rocking for $\nu_{N-C}$, resulting in more than one Fermi resonance. The mixing increases with the chain length increase and the number of Fermi resonances is expected to increase. The coupling of the $\nu_{N\equiv N}$ fundamental and the $\nu_{N=N}$ + $\nu_{N-C}$ combination band, defined from anharmonic calculations with Gaussian 09, is ca. 30 $cm^{-1}$. This value is about three-fold larger than $\beta_{N=N/W}$ or $\beta_{N-C/Ro}$, thus providing no limitations for the mixing. Therefore, the mixing of the $\nu_{N=N}$ and $\nu_{N-C}$ states with the chain states will determine the number of Fermi resonances for the tag. As long as the mixing to chain states occurs, the Fermi resonance will be strong

enough to bring IR intensity to combination bands via intensity borrowing. As a result, the wavepacket on wagging and rocking bands directly initiated by absorbing a photon will require to satisfy the same density of chain state condition at $\nu_{N=N}$ and $\nu_{N-C}$ as the wavepackets following mechanism B. Similarly high transport speed is expected as only a portion of the chain bands will participate in the superposition. The key difference between the mechanisms A and B is that a wavepacket via mechanism A is formed without a delay, while in mechanism B the wavepacket is delayed by the lifetime of the tag. Calculations of the Fermi resonances, performed for the two isotopes (see Section S5 in SI), did not reveal differences that could be related to the experimentally measured speeds reported here. Thus, mechanism A of wavepacket initiation still requires experimental confirmation.

***3.7. Classical modeling of ballistic transport.*** Ballistic energy transport in $N_3C$*n*-a was modeled by solving classical Newton's equations using DFT-determined harmonic force constants (Hessian) (see details in Section S9). Note that harmonic approximation, unsuitable for intramolecular energy redistribution, is expected to work reasonably well for the wavepacket transport. The initial excitation at ca. 1300 $cm^{-1}$ was introduced by exciting a local $\nu_{N=N}$ mode, the relaxation daughter of the $\nu_{N\equiv N}$ tag. Energy arrival to the reporter was monitored by summing all local energies of the carboxylic acid end group atoms. In the absence of energy damping channels, an approximately periodic time dependence was obtained as the excess energy is readily reflected from the chain ends (Fig. 7A). The recurrency period, $t_R$, corresponding to energy round trip, is related to the transport speed as $V = 2L / t_R$, where the chain length, $L$, was taken as $L = n \cdot l_{CC} + l_{NC}$. Here $l_{CC}$ and $l_{NC}$ are the CC and CN bond lengths and $n$ is the number of methylene units in the chain ($n$ = 5, 10, 15).

Comparison of the transport speeds for $^{14}N_3$C5-a and $^{15}N_3$C5-a (Fig. 7A,B) showed that the speed is smaller in $^{15}N_3$C5-a for all chain lengths (Table S5). The averaged speeds of 12 ± 3 Å/ps and 6 ± 1.5 Å/ps was obtained for $^{14}N_3$C*n*-a and $^{15}N_3$C*n*-a, respectively. A damping factor, representing total dephasing of the chain states, was introduced to eliminate the energy arrival recurrencies. The transport speed was found to be somewhat affected by the value of the damping factor. For the damping factor of 1.5 ps (Fig. 7C), a better match with the experimentally observed speeds was found with 13 and 10 Å/ps for $^{14}N_3$C*n*-a and $^{15}N_3$C*n*-a, respectively.

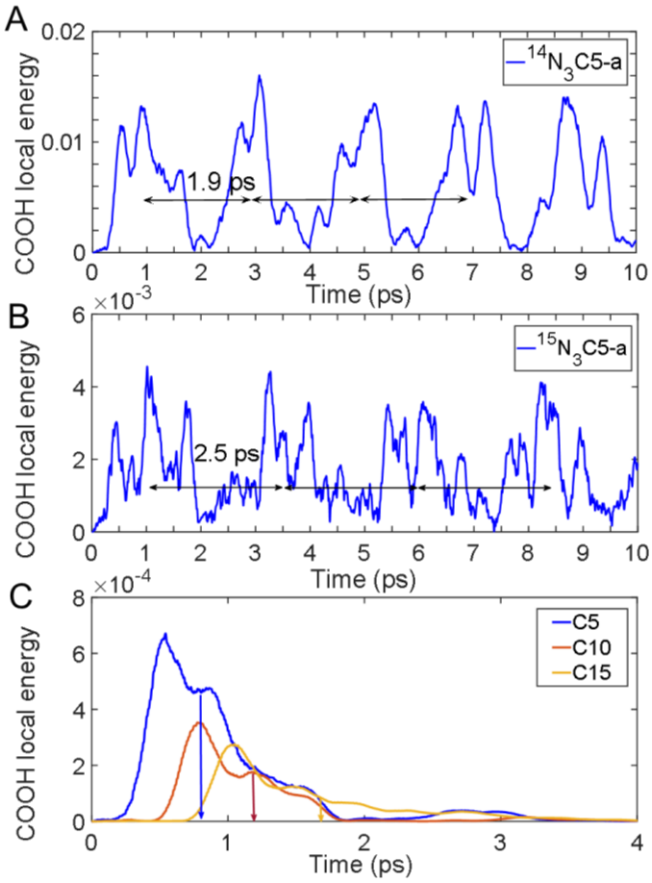


**Fig. 7.** COOH-group local energy vs. time for (A) $^{14}N_3$C5-a, (B) $^{15}N_3$C5-a with infinite damping time and (C) for $^{14}N_3$C*n*-a with the damping time of 1.5 ps and *n* = 5, 10, 15. The color matching arrows show averaged arrival times, $t_D$, calculated using Eq. S5.

## 4. Discussion

Figure 8 summarizes the findings for ballistic transport initiated with $\nu_{N\equiv N}$ in $^{14}N_3$- and $^{15}N_3$- end groups (values for $^{15}N_3$- are shown in parentheses). Mechanism C is found to be contributing the most for both isotopes. The dominant wavepacket propagates via twisting band with the speed of ca. 10 Å/ps for both isotopes. A spatially broad wavepacket at rocking states is expected (mechanism C), propagating with an extremely high speed, exceeding 60 Å/ps. In addition, mechanisms A and B may contribute to ballistic transport via wagging band; the wavepacket is expected to be spatially broad and feature high speed of ca. 36 Å/ps (section S3 in SI).

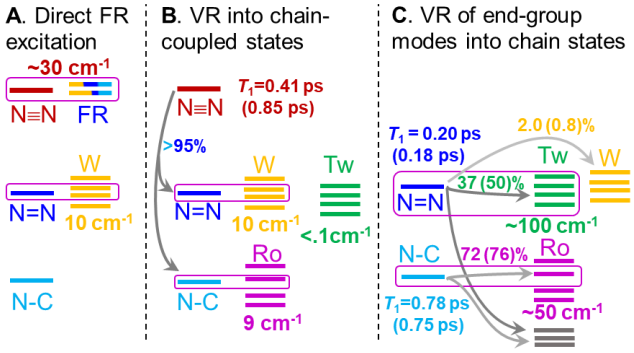

**Fig. 8.** Mechanisms of ballistic transport initiation by excited $\nu_{N\equiv N}$ end group mode. The numbers indicate couplings, if in wavenumbers, lifetimes, if in picoseconds, and rate percent populating band states, if in percent. The values in parentheses computed for $^{15}N_3C5$ follow the values for $^{14}N_3C5$, unless the two values are within a few percent of each other.

$^{14}N_3C5$ and $^{15}N_3C5$ compounds show large similarities in the types of chain bands involved and in the group velocities expected for each band. Two hypotheses are proposed. First, differences in the contributions of various involved wavepackets for the two isotopes determine the overall outcome – faster $V_{Tmax}$ speed for $^{14}N_3C\mathit{n}$-a. Indeed, the formation of the dominant wavepacket on twisting band via mechanism C is more efficient for $^{15}N_3C\mathit{n}$-a (Fig. 8C). This wavepacket defines the $V_{Tmax}$ speed in $^{15}N_3C\mathit{n}$-a. Predicted at 10.4 Å/ps (Table S2 in SI), the speed matches well the experimental value of 11.5 Å/ps in $^{15}N_3C\mathit{n}$-a. Formation of such wavepacket in $^{14}N_3C\mathit{n}$-a is less efficient (Fig. 8C) and faster wavepackets may affect the overall transport more significantly, resulting in a faster $T_{max}$ and $T_{0.8}$ speeds and smaller $T_{max}$ values observed experimentally.

Alternatively, the slower transport speed in $^{15}N_3C\mathit{n}$-a maybe due to a lower group velocity of the dominant wavepacket on the twisting band due to a larger involvement of a higher energy states of the band. Such statement sounds counterintuitive as the $\nu_{N=N}$ frequency shifts down in $^{15}N_3C\mathit{n}$-a. However, as a result of such shift, the $\nu_{N=N}$ relaxation process in $^{14}N_3C\mathit{n}$-a occurs predominantly downhill ($i\rightarrow j+k$), while there is a larger contribution from uphill, $i+k\rightarrow j$ channels in $\nu_{N=N}\rightarrow$Tw relaxation in $^{15}N_3C\mathit{n}$-a (Fig. 5D). The efficiency of the uphill process depends linearly on the population of mode $k$. Compounds with larger chain length feature lower frequencies of acoustic modes, which will be populated thermally to larger quantum numbers and offer increased rate contributions in $\nu_{N=N}\rightarrow$Tw relaxation. At the same time, the twisting states involved in uphill relaxation correspond to the top of the twisting chain band and feature smaller local group velocity. Note that the downhill relaxation channels, $i\rightarrow j+k$, are less sensitive to the energy values of modes $k$, so their rates are not expected to change much for compounds with longer chains. We hypothesize that significantly larger contribution of uphill relaxation channels in $^{15}N_3C5$ results in a smaller mean speed of the wavepacket on the twisting band. A significant difference in the $\nu_{N\equiv N}$ lifetime of ca. 0.4 ps was computed for $^{14}N_3C\mathit{n}$-a (Fig. 8A). However, experimentally measured lifetimes for the two isotopes did not support this prediction, showing similar lifetimes for the two isotopes (Fig. S6 in SI).

No significant mixing among $\nu_{N=N}$ and the twisting modes were found when the azido group is attached to the chain in an anti conformation, which is energetically favorable over gauche conformation, but only by ca. 96 $cm^{-1}$. In the gauche conformation of $N_3$ attachment, $\beta_{N=N/Tw}$ has similar values to $\beta_{N=N/W}$, both are ca. 10 $cm^{-1}$. Note that the anti kink at the azido-group side of the chain results in mixing the identities of the delocalized chain states and inability to assign them as purely wagging or twisting. The treatment of such, less regular but still delocalized states will be considered elsewhere. Nevertheless, the mixing of $\nu_{N=N}$ is still small enough so i) longer chains are required to form the wavepacket efficiently, ii) the expected transport speed corresponds to that of the fast portion of the original wagging and twisting bands, which exceed few folds the experimentally observed speed.

***4.1. General design considerations.*** The analysis of the transport initiation mechanisms in $N_3C\mathit{n}$ revealed that while there is a dominant initiation pathway for shorter chains (mechanism C on twisting band), other mechanisms are expected to contribute more efficiently for longer chains. Higher density of chain states for longer chains is expected to result in a more efficient wavepacket formation on the wagging band *via* mechanism B and A. If this happens, the transport speed will change to that corresponding a local $\frac{d\omega}{dq}$ derivative for the wagging band at the $\nu_{N=N}$ frequency, which is ~36 Å/ps; this switch is expected for chain lengths exceeding $n$ ~ 30 methylene units. A further increase of the transport

speed is expected for even longer compounds with $n$ > 40 units with a larger contribution of a wavepacket on rocking states with the speed ($\frac{d\omega}{dq}$) of ca. 65 Å/ps.

Note also that it is advantageous to use only a portion of the chain band for a wavepacket as such portions often feature almost a linear relation between the frequency and the wavevector, as the case for the wagging and rocking bands at the positions of $\nu_{N=N}$ and $\nu_{N-C}$, respectively. If a linear relation between the frequency and wavevector is satisfied ($\omega \sim q$ + constant), the wavepacket will propagate without much broadening, similar to propagation of a short laser pulse in vacuum, $\omega = cq$, where $c$ is the speed of light in vacuum. On the contrary, a wave packet broadening is expected with time if the whole chain band is involved in the wavepacket.[28]

For one-dimensional chains, chain state localization is expected at some length, which will limit the coherence length for the wavepacket and thus the ballistic transport distance.[29-30] Such localization will occur more readily for the states of narrow bands featuring smaller coupling among unit cells. The chain state localization depends on intramolecular fluctuations as well as on interactions with the solvent.[22] Intramolecular fluctuations include slow conformational variations, such as anti-gauche variations and fast thermal fluctuations. For broad alkane chain bands, such as wagging and rocking, the chain width exceeds many folds the width of the inhomogeneous chain site frequency distribution, which increases the length for chain state localization. Further studies with longer compound are required to understand the extent of the localization.

**Conclusions**

Different mechanisms of ballistic energy transport initiation in oligomeric molecular chains are discussed and tested for transport initiation with $\nu_{N\equiv N}$ excitation in $^{14}N_3C$*n*-a and $^{15}N_3C$*n*-a compounds. We concluded that the dominant mechanism of wavepacket formation in relatively short compounds with $n$ = 5, 10, and 15 involves a two-step relaxation into the twisting band states (mechanism C). While the wavepacket via twisting band dominates the transport, multiple wavepackets involving different optical chain bands and transport speeds are found for both $^{14}N_3C$*n*-a and $^{15}N_3C$*n*-a compounds. The difference in the speed for the two isotopes is linked to a larger contribution of fast wavepackets for $^{14}N_3C$*n*-a.

We concluded that the density of chains states in the studied chains ($n \leq 15$) is insufficient to induce efficient wavepackets at wagging and rocking bands via mechanisms A and B. These mechanisms may become dominant for longer chain offering significantly faster speeds of ca. 36 Å/ps via wagging and ca. 60 Å/ps via rocking bands. The study provides tools for analyzing ballistic transport initiation mechanisms in different molecular systems, which can lead to designing systems featuring efficient initiating and efficient through-chain transport.

The ballistic transport was initiated in this study with mid-IR photon absorption. However, in the case $\nu_{N\equiv N}$ is excited by other means, such as thermally or as a result of electronic relaxation, its relaxation will initiate the same wavepackets in the chain transporting a significant portion of its energy rapidly to large distances along the alkane chain. Optimization of the energy injection and transport efficiencies can help in developing novel materials suitable for energy management and materials for molecular electronics.

**Acknowledgments.** Support by the National Science Foundation (CHE-1900568) is gratefully acknowledged.

**Supplementary Information.** Supporting information includes additional cross peak data and details of their treatment, analysis of the Fermi resonances, dispersion curves for alkyl chains, lifetime data for $\nu_{N\equiv N}$, and vibrational relaxation pathways for $\nu_{N-C}$.

**References**

1. Lin, Z.; Rubtsov, I. V., Constant-speed vibrational signaling along polyethyleneglycol chain up to 60-Å distance. *Proc. Natl. Acad. Sci. U.S.A.* **2012,** *109* (5), 1413-1418.
2. Rubtsova, N. I.; Nyby, C. M.; Zhang, H.; Zhang, B.; Zhou, X.; Jayawickramarajah, J.; Burin, A. L.; Rubtsov, I. V., Room-temperature ballistic energy transport in molecules with repeating units *J. Chem. Phys.* **2015,** *142*, 212412.
3. Rubtsova, N. I.; Qasim, L., N.; Kurnosov, A. A.; Burin, A. L.; Rubtsov, I. V., Ballistic energy transport in oligomers. *Acc. Chem. Res.* **2015,** *48*, 2547-2555.
4. Rubtsov, I. V.; Burin, A. L., Ballistic and diffusive vibrational energy transport in molecules. *J. Chem. Phys.* **2019,** *150* (2), 020901(1-18).
5. Schmitz, A. J.; Pandey, H. D.; Chalyavi, F.; Shi, T.; Fenlon, E. E.; Brewer, S. H.; Leitner, D. M.; Tucker, M. J., Tuning Molecular Vibrational Energy Flow within an Aromatic Scaffold via Anharmonic Coupling. *J. Phys. Chem. A* **2019,** *123* (49), 10571-10581.
6. Fujisaki, H.; Yagi, K.; Kikuchi, H.; Takami, T.; Stock, G., Vibrational energy transport in acetylbenzonitrile described by an ab initio-based quantum tier model. *Chem. Phys.* **2017,** *482*, 86-92.
7. Rubtsova, N. I.; Rubtsov, I. V., Vibrational energy transport in molecules studied by relaxation-assisted two-dimensional infrared spectroscopy. *Ann. Rev. Phys. Chem.* **2015,** *66*, 717-738.
8. Backus, E. H. G.; Nguyen, P. H.; Botan, V.; Pfister, R.; Moretto, A.; Crisma, M.; Toniolo, C.; Stock, G.; Hamm, P., Energy Transport in Peptide Helices: A Comparison between High- and Low-Energy excitation. *J. Phys. Chem.* **2008,** *112*, 9091-9099.
9. Yue, Y.; Qasim, L. N.; Kurnosov, A. A.; Rubtsova, N. I.; Mackin, R. T.; Zhang, H.; Zhang, B.; Zhou, X.; Jayawickramarajah, J.; Burin, A. L.; Rubtsov, I. V., Band-selective ballistic energy transport in alkane oligomers: toward controlling the transport speed. *J. Phys. Chem. B* **2015,** *119* (21), 6448-56.
10. Qasim, L. N.; Atuk, E. B.; Maksymov, A. O.; Jayawickramarajah, J.; Burin, A. L.; Rubtsov, I. V., Ballistic Transport of Vibrational Energy through an Amide Group Bridging Alkyl Chains. *J. Phys. Chem. C* **2019,** *123*, 3381-3392.
11. Schwarzer, D.; Kutne, P.; Schroeder, C.; Troe, J., Intramolecular vibrational energy redistribution in bridged azulene-anthracene compounds: Ballistic energy transport through molecular chains. *J. Chem. Phys.* **2004,** *121* (4), 1754-1764.
12. Schwarzer, D.; Hanisch, C.; Kutne, P.; Troe, J., Vibrational Energy Transfer in Highly Excited Bridged Azulene-Aryl Compounds: Direct Observation of Energy Flow through Aliphatic Chains and into the Solvent. *J. Phys. Chem. A* **2002,** *106* (35), 8019-8028.
13. Wang, Z.; Carter, J. A.; Lagutchev, A.; Koh, Y. K.; Seong, N.-H.; Cahill, D. G.; Dlott, D. D., Ultrafast flash thermal conductance of molecular chains. *Science* **2007,** *317*, 787-790.
14. Wang, Z.; Cahill, D. G.; Carter, J. A.; Koh, Y. K.; Lagutchev, A.; Seong, N.-H.; Dlott, D. D., Ultrafast dynamics of heat flow across molecules. *Chem. Phys.* **2008,** *350*, 31-44.
15. Qasim, L. N.; Kurnosov, A. A.; Yue, Y.; Lin, Z.; Burin, A. L.; Rubtsov, I. V., Energy transport in PEG oligomers: Contributions of different optical bands. *J. Phys. Chem. C.* **2016,** *120* (47), 26663.
16. Rubtsova, N. I.; Rubtsov, I. V., Ballistic energy transport via perfluoroalkane linkers. *Chem. Phys.* **2013,** *422*, 16-21.
17. Leong, T. X.; Qasim, L. N.; Mackin, R. T.; Du, Y.; Jr., R. A. P.; Rubtsov, I. V., Unidirectional coherent energy transport via conjugated oligo(p-phenylene) chains. *J. Chem. Phys.* **2021,** *154* (13), 134304.
18. Leger, J.; Nyby, C.; Varner, C.; Tang, J.; Rubtsova, N. I.; Yue, Y.; Kireev, V.; Burtsev, V.; Qasim, L.; Rubtsov, G. I.; Rubtsov, I. V., Fully automated dual-frequency three-pulse-echo 2DIR spectrometer accessing spectral range from 800 to 4000 wavenumbers. *Rev. Sci. Instr.* **2014,** *85*, 083109.

19. Nyby, C. M.; Leger, J. D.; Tang, J.; Varner, C.; Kireev, V. V.; Rubtsov, I. V., Mid-IR beam direction stabilization scheme for vibrational spectroscopy, including dual-frequency 2DIR. *Opt. Express* **2014,** *22* (6), 6801-6809.
20. Burin, A. L.; Tesar, S. L.; Kasyanenko, V. M.; Rubtsov, I. V.; Rubtsov, G. I., Semiclassical model for vibrational dynamics of polyatomic molecules: Investigation of Internal Vibrational Relaxation. *J. Phys. Chem. C* **2010,** *114* (48), 20510-20517.
21. Tesar, S. L.; Kasyanenko, V. M.; Rubtsov, I. V.; Rubtsov, G. I.; Burin, A. L., Theoretical study of internal vibrational relaxation and energy transport in polyatomic molecules. *J. Phys. Chem. A* **2013,** *117* (2), 315-323.
22. Rubtsova, N. I.; Lin, Z.; Mackin, R. T.; Rubtsov, I. V., How Intramolecular Vibrational Energy Transport Changes with Rigidity and Polarity of the Environment? *High Energy Chem.* **2020,** *54* (6), 427–435.
23. Varner, C.; Zhou, X.; Saxman, Z. K.; Leger, J. D.; Jayawickramarajah, J.; Rubtsov, I. V., Azido alkanes as convenient reporters for mobility within lipid membranes. *Chem. Phys.* **2018,** *512*, 20-26.
24. Gruebele, M.; Wolynes, P. G., Vibrational energy flow and chemical reactions. *Acc. Chem. Res.* **2004,** *37* (4), 261-7.
25. Leitner, D. M., Thermal Boundary Conductance and Thermal Rectification in Molecules. *J. Phys. Chem. B* **2013,** *117* 12820-12828.
26. Pandey, H. D.; Leitner, D. M., Thermalization and Thermal Transport in Molecules. *J. Phys. Chem. Lett.* **2016,** *7* (24), 5062-5067.
27. Frisch, M. J.; Trucks, G. W.; Schlegel, H. B.; Scuseria, G. E.; Robb, M. A.; Cheeseman, J. R.; Montgomery, J. A.; T. Vreven, J.; Kudin, K. N.; Burant, J. C.; Millam, J. M.; Iyengar, S. S.; Tomasi, J.; Barone, V.; Mennucci, B.; Cossi, M.; Scalmani, G.; Rega, N.; Petersson, G. A.; Nakatsuji, H.; Hada, M.; Ehara, M.; Toyota, K.; Fukuda, R.; Hasegawa, J.; Ishida, M.; Nakajima, T.; Honda, Y.; Kitao, O.; Nakai, H.; Klene, M.; Li, X.; Knox, J. E.; Hratchian, H. P.; Cross, J. B.; Bakken, V.; Adamo, C.; Jaramillo, J.; Gomperts, R.; Stratmann, R. E.; Yazyev, O.; Austin, A. J.; Cammi, R.; Pomelli, C.; Ochterski, J. W.; Ayala, P. Y.; Morokuma, K.; Voth, G. A.; Salvador, P.; Dannenberg, J. J.; Zakrzewski, V. G.; Dapprich, S.; Daniels, A. D.; Strain, M. C.; Farkas, O.; Malick, D. K.; Rabuck, A. D.; Raghavachari, K.; Foresman, J. B.; Ortiz, J. V.; Cui, Q.; Baboul, A. G.; Clifford, S.; Cioslowski, J.; Stefanov, B. B.; Liu, G.; Liashenko, A.; Piskorz, P.; I. Komaromi, R. L. M., D. J. Fox, T. Keith, M. A. Al-Laham, ; C. Y. Peng, A. N., M. Challacombe, P. M. W. Gill, ; B. Johnson, W. C., M. W. Wong, C. Gonzalez, and J. A. Pople, *Gaussian 09, Revision A.02, Gaussian, Inc., Wallingford CT* **2009**.
28. Fayer, M. D., *Elements of quantum mechanics*. Oxford University Press: 2001; p 356.
29. Anderson, P. W., Absence of Diffusion in Certain Random Lattices. *Physical Review* **1958,** *109* (5), 1492-1505.
30. Juntunen, T.; Vänskä, O.; Tittonen, I., Anderson Localization Quenches Thermal Transport in Aperiodic Superlattices. *Physical review letters* **2019,** *122* (10), 105901.